A Symmetric FEM-IE Formulation With a Single-Level IE-QR Algorithm for Solving Electromagnetic Radiation and Scattering Problems

Marinos N. Vouvakis, *Student Member, IEEE*, Seung-Cheol Lee, Kezhong Zhao, and Jin-Fa Lee, *Senior Member, IEEE*

***Abstract*—This paper presents, for the first time in the engineering community, a symmetric coupling between the finite element and integral equation methods (FEM-IE) for solving three-dimensional unbounded radiation and scattering problems. The proposed FEM-IE is based on the E-field vector Helmholtz equation. Curl-conforming vector finite elements are used to discretize the interior region, whereas the divergence-conforming surface elements are utilized in the IE truncation surface. The symmetry in the IE part is restored through the application of the *Calderon-projector*. Moreover, the IE computations are accelerated using a single level QR algorithm. This reduces both memory and computational time. Furthermore it allows the use of different Green's functions for the exterior problem, with only minor modifications on the algorithm. The resulted system of equations is solved with a very efficient preconditioned conjugate gradient (PCCG) with a p-Multiplicative Schwarz preconditioner.**

***Index Terms*—Fast integral equation method, hybrid finite element method and integral equation method, multiplicative Schwarz preconditioner, radiation and scattering.**

I. Introduction

THE finite element method-integral equation method (FEM-IE) is one of the most appealing methods for the analysis of unbounded electromagnetic problems such as antenna radiation and radar cross-section (RCS) computations. Despite its accuracy advantages over other methods, it has two major drawbacks. The matrix resulting from the coupling of the two methods, usually leads to a nonsymmetric system of equations [1]. This naturally increases the computation time for assembling the dense IE submatrix and doubles the memory requirements. Moreover, due to the lack of effective and efficient preconditioners, the resulting FEM-IE matrix equations are usually solved using direct solution techniques [1]–[3]. In [3], Liu and Jin proposed the use of the direct factorization of the FEM-absorbing boundary condition (ABC) matrix as the preconditioner for the FEM-IE formulation. The approach is effective but not very efficient, since it requires a direct factorization of the FEM-ABC matrix; for general problems, the computational complexity can exceed $O(N^{7/3})$, where N is the number of FEM unknowns. For some special problem geometries, direct solution techniques, such as multifrontal methods [1], can outperform iterative matrix solution methods. However, in general, when an effective and efficient preconditioner is found, iterative matrix solution approach is the choice for large size problems both in terms of memory and CPU time. The second major limitation of FEM-IE has to do with the memory and computational effort required to assemble the dense IE matrix block. In a problem with N_s IE unknowns, both the storage and the CPU time for a single matrix vector product are of $O(N_s^2)$, assuming iterative matrix solution is employed.

Both weaknesses of the FEM-IE method seem to be major bottleneck of the FEM-IE in the quest for solving electrically large radiation and scattering problems.

In this paper both drawbacks of the "conventional" FEM-IE are tackled. The approach is based on a novel *symmetric* coupling between finite element and integral equation methods. The major building blocks of the current approach are:

1) a symmetric hybrid FEM-IE formulation is proposed which is based on the employment of the *Calderon-projector* [4];

2) a single-level IE-QR algorithm [5], which is a low-rank matrix representation, is adopted to achieve $O(N_s^{1.5})$ complexity for moderate size problems;

3) the resulting single-level IE-QR algorithm will be employed in conjunction with the symmetric FEM-IE formulation to significantly speed up the formation as well as matrix-vector multiplication of the dense integral equation portion;

4) A p-type Multiplicative Schwarz (p-MUS) [6]–[8] preconditioner, which has been developed previously for solving the FEM matrix equations arisen from Maxwell equations using hierarchical curl-conforming basis functions, is extended and modified to solve the resulting symmetric complex matrix equation of the hybrid FEM-IE formulation.

The inspiration of this paper is originated from the previously understated work of Hoppe [9] and the recent work by Hiptmair in [10]. In the case of [9], a modified version of the present FEM-IE was applied for the solution of electromagnetic scattering by a body of revolution. The major difference

Manuscript received October 4, 2003; revised February 21, 2004. This work was supported in part by Ansoft Corporation through two Ansoft fellowships and in part by Temasek Laboratory, National University of Singapore, Singapore.

The authors are with the ElectroScience Laboratory, Electrical Engineering Department, The Ohio State University, Columbus, OH 43212-1191 USA (e-mail: vouvakis.1@osu.edu; lee.1802@osu.edu; zhaoed@yahoo.com; lee.1863@osu.edu).

Digital Object Identifier 10.1109/TAP.2004.837525

between this work and [9] is that now only a set of extra surface current unknowns is needed. Hiptmair in [10] applied the present method with a slightly modified testing procedure for low-frequency eddy current problems. The first to carry out the symmetric coupling of the FEM-IE seem to be Costabel [11], [12]. The method was initially developed for elliptic problems such as electrostatics and elastoplastic problems. Following the work of Costabel, Ammari and Nedelec theoretically analyzed the method for electromagnetic problems in [13]. In electromagnetics community none of the available hybridizations have managed to retain the symmetry of the final FEM-IE system [1]–[3] and [14]–[16]. This paper is the first attempt to implement and put in practice the theoretical developments of the mathematical community.

The rest of this paper is structured as follows. Section II is the core of the paper; after a short introduction to the notations, it describes in detail the theoretical development that leads to the symmetric coupling. In Section III a summary of the IE-QR algorithm described in [5] is given. An extension to the FEM-IE of the effective preconditioner of [6]–[8] is presented in Section IV. The numerical results of this work are presented in Section V. Finally, some concluding remarks and look ahead are given in Section VI.

II. Symmetric Coupling of FEM-IE

A. Boundary Value Problem

Before start developing the theory and formulation of the symmetric coupling between FEM and IE, it is essential to introduce some notations and definitions that will ease the reading of this section. Throughout the manuscript, boldface capital letters will represent matrices, except when explicitly stated otherwise; boldface lowercase letters represent column/row vectors. The overhead arrow notation will be reserved for vector fields, and hat, e.g., $\hat{a}$ indicates unit vector in $\mathbb{R}^3$. Position vectors $\vec{r}$ and $\vec{r}'$ refer to the observation and source, respectively.

Most of the definitions will be loosely presented for the sake of brevity and clarity; for rigorous definitions the interested reader is referred to the Ph.D. dissertation of Buffa [17]. First let us define the surface integral of two complex-valued vector functions as

$$\langle \vec{u}, \vec{v} \rangle_\Gamma = \int_\Gamma \vec{u} \bullet \vec{v} d\Gamma. \tag{1}$$

Similarly, the volume integral of two complex valued functions in a domain Ω. is denoted by

$$\langle \vec{u}, \vec{v} \rangle_\Omega = \int_\Omega \vec{u} \bullet \vec{v} d\Omega. \tag{2}$$

Several spaces need to be defined beforehand. The following convention will be adopted: spaces of scalar valued functions will be denoted by H, whereas for spaces of vector valued functions the boldface letter $\mathbf{H}$ will be used. One of the most important spaces in electromagnetics is that of curl-conforming functions in a subdomain Ω

$$\mathbf{H}(curl, \Omega) = \left\{ u \left| \int_\Omega \left(|\nabla \times \vec{u}|^2 + |\vec{u}|^2 \right) d\Omega < \infty \right. \right\}. \tag{3}$$

This is the space where electric and magnetic fields reside; the physical meaning of the space $\mathbf{H}(curl, \Omega)$ is that in subdomain Ω, the electric and magnetic energies are finite. Now it is time to introduce some trace operators and spaces of tangential vector fields on the surface $\Gamma = \partial\Omega$. First let us define the *tangential surface trace* γ_t acting on $\vec{u}$ as

$$\gamma_t \vec{u} := \hat{n} \times (\vec{u} \times \hat{n}) \tag{4}$$

where $\hat{n}$ denotes the outward pointing unit vector on surface Γ. In other words, $\gamma_t \vec{u}$ contains the tangential components of the vector field $\vec{u}$ on the surface Γ. A second trace necessary for the definition of the integral equations is the *twisted tangential trace* $\gamma_t^\times$ which is defined as

$$\gamma_t^\times \vec{u} := \hat{n} \times \vec{u} \tag{5}$$

which again implies that $\gamma_t^\times \vec{u}$, contains the tangential components of $\vec{u}$ on surface Γ, the same as $\gamma_t \vec{u}$, but twisted 90° around $\hat{n}$.

Of particular interest in this work will be the spaces $\mathbf{H}_{||}^{1/2}(\Gamma)$ and $\mathbf{H}_{\perp}^{1/2}(\Gamma)$ of surface vector functions on Γ. Informally speaking, these spaces contain the tangential surface vector fields with "weak tangential continuity" and "weak normal continuity," respectively, across the edges of a faceted surface Γ. The exact definitions of these spaces can be found in [17]. It is important to emphasize the weak nature of the continuity, since the surface can be faceted; in that case, strong continuity along the edges and corners cannot be rigorously defined. The corresponding dual spaces of $\mathbf{H}_{||}^{1/2}$ and $\mathbf{H}_{\perp}^{1/2}$ will be denoted by $\mathbf{H}_{||}^{-1/2}$ and $\mathbf{H}_{\perp}^{-1/2}$, respectively; again for the definition of the dual space we suggest the readers to consult any functional analysis book such as [18]. Finally, and most important for this work, the following two spaces need to be defined

$$\mathbf{H}_{||}^{-\frac{1}{2}}(div_\Gamma, \Gamma) = \left\{ \vec{u} \in \mathbf{H}_{||}^{-\frac{1}{2}}(\Gamma), \nabla_\Gamma \bullet \vec{u} \in H^{-\frac{1}{2}}(\Gamma) \right\} \tag{6}$$

and

$$\mathbf{H}_{\perp}^{-\frac{1}{2}}(curl_\Gamma, \Gamma) = \left\{ \vec{u} \in \mathbf{H}_{\perp}^{-\frac{1}{2}}(\Gamma), \nabla_\Gamma \times \vec{u} \in H^{-\frac{1}{2}}(\Gamma) \right\} \tag{7}$$

where $\nabla_\Gamma \bullet$ and $\nabla_\Gamma \times$ are the surface divergence and curl operators defined in [4]. From engineering point of view, it is sufficient to say $\mathbf{H}_{||}^{-1/2}(div_\Gamma, \Gamma)$ is the space that the RWG belong to; similarly, $\mathbf{H}_{\perp}^{-1/2}(curl_\Gamma, \Gamma)$ contains the surface Whitney 1-form (or edge elements). The following theorem, taken directly from [17], helps to establish the trial and test function spaces for the symmetric coupling of the FEM and IE.

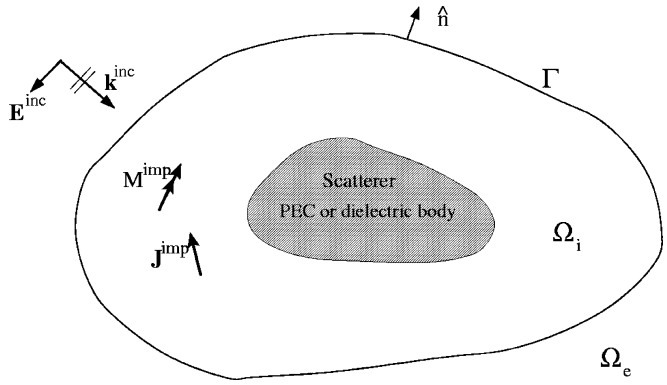

Fig. 1. Generic geometry of a scatterer.

Trace Theorem: The trace mapping $\gamma_t : \mathbf{H}(curl,\Omega) \mapsto \mathbf{H}_{\perp}^{-1/2}(curl_{\Gamma},\Gamma)$ and $\gamma_t^{\times} : \mathbf{H}(curl,\Omega) \mapsto \mathbf{H}_{\|}^{-1/2}(div_{\Gamma},\Gamma)$ are linear and continuous.

It is very important at this point to note that $\mathbf{H}_{\perp}^{-1/2}(curl_{\Gamma},\Gamma)$ and $\mathbf{H}_{\|}^{-1/2}(div_{\Gamma},\Gamma)$ are *dual* to each other through a duality pairing defined by (1). That is to say

$$\left(\mathbf{H}_{\|}^{-\frac{1}{2}}(div_{\Gamma},\Gamma)\right)' = \mathbf{H}_{\perp}^{-\frac{1}{2}}(curl_{\Gamma},\Gamma) \tag{8}$$

where prime indicates the dual space.

Referring to Fig. 1 let Ω_i be a regular bounded domain in $\mathbb{R}^3$ that contains the scatterer or antenna of interest. A second exterior domain Ω_e is naturally defined as $\Omega_e = \mathbb{R}^3 \setminus \overline{\Omega}_i$. The two domains are separated by a regular closed surface $\Gamma = \partial\Omega_i$ which can conform to the shape of the scatterer. The exterior and interior sides of the surface Γ will be denoted by Γ^+ and Γ^-, respectively. The unit normal vector $\hat{n}$ on Γ is assumed to point toward the exterior region. We consider the electromagnetic radiation and/or scattering problems in the presence of a dielectric or conducting medium of arbitrary shape. In the case of radiation, the sources of electromagnetic field are $\vec{J}^{\rm imp}$ and $\vec{M}^{\rm imp}$ residing in Ω_i. On the other hand, in the scattering case the sources are assumed to exist somewhere in Ω_e and produce locally on Γ a plane wave of the form $\vec{E}^{\rm inc}(\vec{r}) = \vec{E}_0 e^{-j\vec{k}^{\rm inc}\cdot\vec{r}}$. $\vec{E}_0$ and $\vec{k}^{\rm inc}$ are the incident electric field vector and vector wave number, respectively. The material surrounding the scatterer is assumed to be air, with wavenumber $k_0 = \omega\sqrt{\mu_0\varepsilon_0}$.

The boundary value problem (BVP) statement for the configuration of Fig. 1 reads

Find an electric field $\vec{\rm E}$ that satisfies the system

$$\left.\begin{array}{c} \nabla\times\frac{1}{\mu_r}\nabla\times\vec{E} - k_0^2\varepsilon_r\vec{E} = -j\omega\mu_o\vec{j}^{\rm imp} \quad \text{in } \Omega_i \\ \nabla\times\nabla\times\vec{E} - k_0^2\vec{E} = -j\omega\mu_o\vec{j}^{\rm inc} \quad \text{in } \Omega_e \\ \gamma_t^{\times}\vec{E}|_{\Gamma^-} = \gamma_t^{\times}\vec{E}|_{\Gamma^+} \\ \frac{1}{\mu_r^-}\gamma_t^{\times}(\nabla\times\vec{E})\Big|_{\Gamma^-} = \frac{1}{\mu_r^+}\gamma_t^{\times}(\nabla\times\vec{E})\Big|_{\Gamma^+} \\ \lim\limits_{r\to\infty}|\vec{r}|[(\nabla\times\vec{E})\times\frac{\vec{r}}{|\vec{r}|} - jk_0\vec{E}] = 0 \end{array}\right\} \tag{9}$$

where the last equation in (9) is the Silver–Muller radiation condition. In addition, μ_r^- and μ_r^+ are the relative permeabilities of the materials on either side of Γ; also $\vec{J}^{\rm inc}$ is the current producing the incident field $\vec{E}^{\rm inc}$ in the exterior region Ω_e.

a) Representation formulae for the exterior region: A proper coupling between FEM and IE should start with the appropriate representation formulae for the fields in the exterior region Ω_e. Associated with the problem of (9), the following representation formulae for electric and magnetic fields in the exterior region Ω_e are obtained [4]:

$$\begin{aligned} \vec{E}(\vec{r}) = \vec{E}^{\rm inc}(\vec{r}) &+ \int_{\Gamma}\vec{j}(\vec{r}')g(\vec{r}|\vec{r}')d\Gamma' \\ &+ \frac{1}{k_0^2}\nabla\int_{\Gamma}\nabla_{\Gamma}'\bullet\vec{j}(\vec{r}')g(\vec{r}|\vec{r}')d\Gamma' \\ &+ \nabla\times\int_{\Gamma}\vec{m}(\vec{r}')g(\vec{r}|\vec{r}')d\Gamma' \end{aligned} \tag{10}$$

$$\begin{aligned} -j\omega\mu_0\vec{H}(\vec{r}) = -j\omega\mu_0\vec{H}^{\rm inc}(\vec{r}) &+ k_0^2\int_{\Gamma}\vec{m}(\vec{r}')g(\vec{r}|\vec{r}')d\Gamma' \\ &+ \nabla\int_{\Gamma}\nabla_{\Gamma}'\bullet\vec{m}(\vec{r}')g(\vec{r}|\vec{r}')d\Gamma' \\ &+ \nabla\times\int_{\Gamma}\vec{j}(\vec{r}')g(\vec{r}|\vec{r}')d\Gamma' \end{aligned} \tag{11}$$

where $\vec{r}\in\Omega_e$, $\vec{m} = \gamma_t^{\times}\vec{E}$ and $\vec{j} = (1/\mu_r)\gamma_t^{\times}(\nabla\times\vec{E})$. The Green's function $g(\vec{r}|\vec{r}')$ is that of the free-space given by

$$g(\vec{r}|\vec{r}') = \frac{e^{-jk|\vec{r}-\vec{r}'|}}{4\pi|\vec{r}-\vec{r}'|}. \tag{12}$$

It should be noted that $\vec{E}(\vec{r})$ and $\vec{H}(\vec{r})$ belong to the curl-conforming vector space, i.e., $\vec{E} \in \mathbf{H}(curl,\Omega_e)$ and $\vec{H} \in \mathbf{H}(curl,\Omega_e)$.

To obtain a set of independent integral equations from the integral representations of (10) and (11) one allows $\vec{r}\to\Gamma^+$. Thus, taking the tangential surface trace γ_t of (10), and the twisted tangential trace $\gamma_t^{\times}$ of (11), results in

$$\begin{aligned} \frac{1}{2}\vec{e}(\vec{r}) = \vec{e}^{\rm inc}(\vec{r}) &+ \gamma_t{\rm pv}\int_{\Gamma}\vec{m}(\vec{r}')\times\nabla'g(\vec{r}|\vec{r}')d\Gamma' \\ &+ \frac{1}{k_0^2}\nabla_{\Gamma}\int_{\Gamma}\nabla_{\Gamma}'\bullet\vec{j}(\vec{r}')g(\vec{r}|\vec{r}')d\Gamma' \\ &+ \gamma_t\int_{\Gamma}\vec{j}(\vec{r}')g(\vec{r}|\vec{r}')d\Gamma' \end{aligned} \tag{13}$$

$$\begin{aligned} \frac{1}{2}\vec{j}(\vec{r}) = \vec{j}^{\rm inc}(\vec{r}) &+ k_0^2\gamma_t^{\times}\int_{\Gamma}\vec{m}(\vec{r}')g(\vec{r}|\vec{r}')d\Gamma' \\ &+ \gamma_t^{\times}\nabla\int_{\Gamma}\nabla_{\Gamma}'\bullet\vec{m}(\vec{r}')g(\vec{r}|\vec{r}')d\Gamma' \\ &+ \gamma_t^{\times}{\rm pv}\int_{\Gamma}\vec{j}(\vec{r}')\times\nabla'g(\vec{r}|\vec{r}')d\Gamma' \end{aligned} \tag{14}$$

where the appropriate principal value evaluation of the hypersingular integrals was employed. The formulas in (13) and (14)

are the expressions corresponding to the exterior Calderon projector. In both (13) and (14), pv denotes integration in the principal value sense. Moreover, the following notation for the tangential electric field was adopted:

$$\vec{e} \equiv \gamma_t \vec{E}. \tag{15}$$

Naturally, from the trace theorem we conclude that $\vec{e} \in \mathbf{H}_{\perp}^{-1/2}(curl_{\Gamma}, \Gamma)$, and $\vec{j} \in \mathbf{H}_{||}^{-1/2}(div_{\Gamma}, \Gamma)$. Equations (13) and (14) are the well known electric field integral equations (EFIE) and magnetic field integral equations (MFIE), respectively.

The weak statement of the above integral equations is obtained by testing each equation with the appropriate set of testing functions. As it will become clear in Section III, the appropriate testing of each integral equation is crucial to retain the symmetry of the FEM-IE formulation. In the current approach, the testing is done through the duality pairing. That is: the appropriate space to test $\vec{e} \in \mathbf{H}_{\perp}^{-1/2}(curl_{\Gamma}, \Gamma)$ is its dual space $\mathbf{H}_{||}^{-1/2}(div_{\Gamma}, \Gamma)$; whereas the appropriate testing space for $\vec{j} \in \mathbf{H}_{||}^{-1/2}(div_{\Gamma}, \Gamma)$ will be its dual space $\mathbf{H}_{\perp}^{-1/2}(curl_{\Gamma}, \Gamma)$. For that reason, the EFIE will be tested by functions that belong to the div-conforming trace space, which is the space of the well-known RWG functions. On the other hand MFIE is tested by surface curl-conforming basis functions on Γ. This leads to

$$\begin{aligned}\frac{1}{2}\langle \vec{\lambda}, \vec{e} \rangle_{\Gamma} &= \langle \vec{\lambda}, \vec{e}^{\,\mathrm{inc}} \rangle_{\Gamma} + \left\langle \vec{\lambda}, \vec{C}(\vec{m}) \right\rangle_{\Gamma} \\ &\quad - \frac{1}{k_0^2} \left\langle \nabla_{\Gamma} \bullet \vec{\lambda}, \Psi(\vec{j}) \right\rangle_{\Gamma} + \left\langle \vec{\lambda}, \vec{A}(\vec{j}) \right\rangle_{\Gamma} \\ &\quad \forall \vec{\lambda} \in \mathbf{H}_{||}^{-\frac{1}{2}}(div_{\Gamma}, \Gamma) \end{aligned} \tag{16}$$

$$\begin{aligned}\frac{1}{2}\langle \vec{v}, \vec{j} \rangle_{\Gamma} &= \langle \vec{v}, \vec{j}^{\,\mathrm{inc}} \rangle_{\Gamma} - \left\langle \hat{n} \times \vec{v}, \vec{C}(\vec{j}) \right\rangle_{\Gamma} \\ &\quad + \langle \nabla_{\Gamma} \bullet (\hat{n} \times \vec{v}), \Psi(\vec{m}) \rangle_{\Gamma} - k_0^2 \left\langle \hat{n} \times \vec{v}, \vec{A}(\vec{m}) \right\rangle_{\Gamma} \\ &\quad \forall \vec{v} \in \mathbf{H}_{\perp}^{-\frac{1}{2}}(curl_{\Gamma}, \Gamma). \end{aligned} \tag{17}$$

In (16) and (17), the following notations were used:

$$\begin{aligned}\vec{A}(\vec{x}) &= \int_{\Gamma} \vec{x}(\vec{r}\,') g(\vec{r}|\vec{r}\,') d\Gamma' \\ \Psi(\vec{x}) &= \int_{\Gamma} \nabla_{\Gamma}' \bullet \vec{x}(\vec{r}\,') g(\vec{r}|\vec{r}\,') d\Gamma' \\ \vec{C}(\vec{x}) &= pv \int_{\Gamma} \vec{x}(\vec{r}\,') \times \nabla' g(\vec{r}|\vec{r}\,') d\Gamma'. \end{aligned} \tag{18}$$

At this point, it is necessary to stress that $\vec{e}$ and $\vec{j}$ on (16) and (17) refer to the field and current just on the exterior of the truncation surface Γ, namely

$$\begin{aligned}\vec{e} &:= \vec{e}^{+} = \vec{e}|_{\Gamma^+} \\ j &:= \vec{j}^{+} = \vec{j}|_{\Gamma^+}. \end{aligned} \tag{19}$$

b) Interior problem: In a traditional manner, the weak statement of interior problem in (9) leads to

$$b(\vec{v}, \vec{E}) + \langle \vec{v}, \vec{j}^{-} \rangle_{\Gamma} = \langle \vec{v}, \vec{J}^{\mathrm{imp}} \rangle_{\Omega_i} \tag{20}$$

were the bilinear form $b(\vec{v}, \vec{E})$ is defined by

$$b(\vec{v}, \vec{E}) = \int_{\Omega_i} \left(\nabla \times \vec{v} \bullet \frac{1}{\mu_r} \nabla \times \vec{E} - k_0^2 \varepsilon_r \vec{v} \bullet \vec{E} \right) d\Omega \tag{21}$$

where $\vec{v}$ is the testing function, and $\vec{j}^{-} = \hat{n} \times (1/\mu_r) \nabla \times \vec{E}|_{\Gamma^-}$ is defined just inside the truncation surface. By enforcing the continuity of the tangential magnetic field on Γ

$$\vec{j}^{-} = \vec{j}^{+} \tag{22}$$

(20) becomes

$$b(\vec{v}, \vec{E}) + \langle \vec{v}, \vec{j}^{+} \rangle_{\Gamma} = \langle \vec{v}, \vec{J}^{\mathrm{imp}} \rangle_{\Omega_i}. \tag{23}$$

c) Coupling: The breakthrough to obtain a symmetric coupling of FEM and IE was accomplished by Costabel in [11] by splitting the surface integral term in (23) into two halves; one half was left intact while substituting the other from (17). This crucial modification, along with the appropriate testing of (16) and (17) permits the symmetric coupling of FEM and IE. In doing so, the following variational formulation is obtained:

$$\left.\begin{aligned} &b(\vec{v}, \vec{E}) + \tfrac{1}{2}\langle \vec{v}, \vec{j} \rangle_{\Gamma} - \left\langle \hat{n} \times \vec{v}, \vec{C}(\vec{j}) \right\rangle_{\Gamma} + \langle \nabla_{\Gamma} \bullet (\hat{n} \times \vec{v}), \Psi(\vec{m}) \rangle_{\Gamma} \\ &\quad - k_0^2 \left\langle \hat{n} \times \vec{v}, \vec{A}(\vec{m}) \right\rangle_{\Gamma} = -\langle \hat{n} \times \vec{v}, \vec{j}^{\,\mathrm{inc}} \rangle_{\Gamma} + \langle \vec{v} \bullet \vec{J}^{\mathrm{imp}} \rangle_{\Omega_i} \\ &\tfrac{1}{2}\langle \vec{\lambda}, \vec{e} \rangle_{\Gamma} - \left\langle \vec{\lambda}, \vec{C}(\vec{m}) \right\rangle_{\Gamma} + \tfrac{1}{k_0^2} \left\langle \nabla_{\Gamma} \bullet \vec{\lambda}, \Psi(\vec{j}) \right\rangle_{\Gamma} \\ &\quad - \left\langle \vec{\lambda}, \vec{A}(\vec{j}) \right\rangle_{\Gamma} = \langle \vec{\lambda}, \vec{e}^{\,\mathrm{inc}} \rangle_{\Gamma} \end{aligned}\right\}. \tag{24}$$

The discretization process proceeds by approximating both $\Omega_i \approx \Omega_i^h = \bigcup_{m=0}^{M_I} T_m^h$ and $\Gamma \approx \Gamma^h = \bigcup_{m=0}^{M_s} \Delta_m^h$ by a set of tetrahedrons T^h and triangles Δ^h of average edge length h. The finite dimensional weak formulation of the BVP can be stated as

Seek $\vec{E}^h \in V^h \subset \mathbf{H}(curl, \Omega_i)$ and $\vec{j}^h \in \Lambda^h \subset \mathbf{H}_{||}^{-\frac{1}{2}}(div_{\Gamma}, \Gamma)$ such that (24) is satisfied for all $\vec{v}^h \in V^h \subset \mathbf{H}(curl, \Omega_i)$ and $\vec{\lambda}^h \in \Lambda^h \subset \mathbf{H}_{||}^{-\frac{1}{2}}(div_{\Gamma}, \Gamma)$.

Notice that in the weak statement, we have already applied the Galerkin treatment. Namely, the trial and testing function spaces are set to be the same. Each space is spanned by the appropriate set of basis functions $\vec{w}$ and $\hat{n} \times \vec{w}$ respectively. That is

$$\begin{aligned}\vec{E}^h &= \sum_{n=0}^{N_I} \vec{w}_n(\vec{r}) e_{i,n} + \sum_{n=N_I}^{N} \vec{w}_n(\vec{r}) e_{s,n}, \quad \vec{w}_n \in V^h \\ \vec{j}^h &= \sum_{n=N_I}^{N} \hat{n} \times \vec{w}_n(\vec{r}) j_{s,n}, \quad \hat{n} \times \vec{w}_n \in \Lambda^h \end{aligned} \tag{25}$$

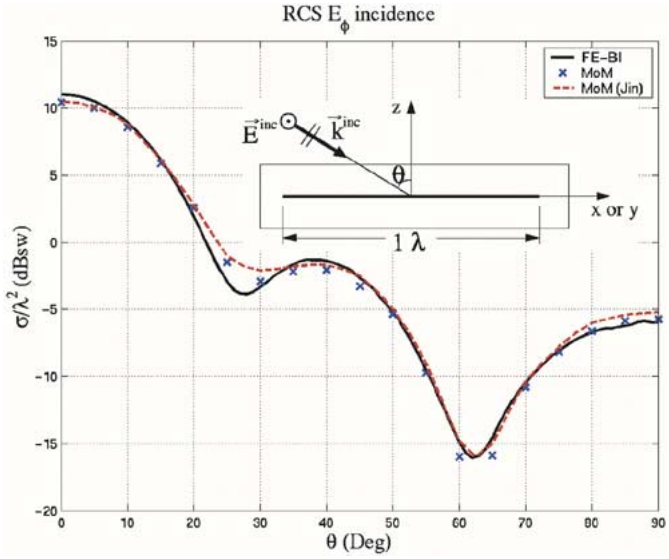

Fig. 2. Monostatic RCS of a $1\lambda \times 1\lambda$ PEC plate under horizontal polarization incidence.

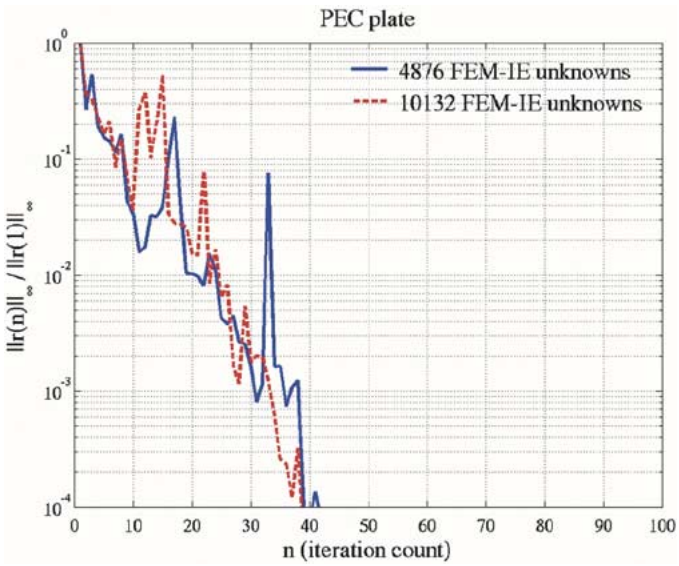

Fig. 3. Normalized ∞-norm residual versus number of iterations of the Schwartz solver for the scattering problem of Fig. 2.

where, $e_{i,n}$ refers to the coefficients inside Ω_i, whereas $e_{s,n}$ and $j_{s,n}$ are the electric field and current coefficients on boundary Γ. In this work $\vec{w}$'s are the $\mathrm{p} = 2$ hierarchical, first-kind Nedelec elements [19]. Combining (24) and (25) the final system of equations is obtained

$$\begin{pmatrix} \mathbf{A} & \mathbf{C} & 0 \\ \mathbf{C}^T & \mathbf{B}+\mathbf{Q}_M & \mathbf{D}+\mathbf{P}_M \\ 0 & \mathbf{D}^T+\mathbf{P}_E & \mathbf{Q}_E \end{pmatrix} \begin{pmatrix} \mathbf{e}_i \\ \mathbf{e}_s \\ \mathbf{j}_s \end{pmatrix} = \begin{pmatrix} \mathbf{b} \\ \mathbf{y}_M \\ \mathbf{y}_E \end{pmatrix} \quad (26)$$

where $\mathbf{A}$, $\mathbf{B}$, and $\mathbf{C}$ are the common FEM sub-blocks [20]. The IE associated matrix sub-blocks are given by

$$\begin{aligned}(\mathbf{Q}_M)_{ij} = &-k_0^2 \int_{S_i} \hat{n} \times \vec{w}_i(\vec{r}) \bullet \int_{S_j} \hat{n}' \times \vec{w}_j(\vec{r}') g(\vec{r}|\vec{r}') d\Gamma' d\Gamma \\ &+ \int_{S_I} \nabla_\Gamma \bullet (\hat{n} \times \vec{w}_i(\vec{r})) \\ &\times \int_{S_j} \nabla'_\Gamma \bullet (\hat{n}' \times \vec{w}_j(\vec{r}')) \, g(\vec{r}|\vec{r}') d\Gamma' d\Gamma \quad (27)\end{aligned}$$

$$(\mathbf{Q}_E)_{ij} = \frac{1}{k_0^2} (\mathbf{Q}_M)_{ij} \quad (28)$$

$$\begin{aligned}(\mathbf{P}_M)_{ij} = &\int_{S_i} \hat{n} \times \vec{w}_i(\vec{r}) \bullet pv \\ &\times \int_{S_j} \hat{n}' \times \vec{w}_j(\vec{r}') \times \nabla g(\vec{r}|\vec{r}') d\Gamma' d\Gamma \quad (29)\end{aligned}$$

$$(\mathbf{P}_E)_{ij} = (\mathbf{P}_M)_{ij} \quad (30)$$

$$\mathbf{D}_{ij} = \frac{1}{2} \int_{S_i \cap S_j} \vec{w}_i(\vec{r}) \bullet \hat{n} \times \vec{w}_j(\vec{r}) d\Gamma. \quad (31)$$

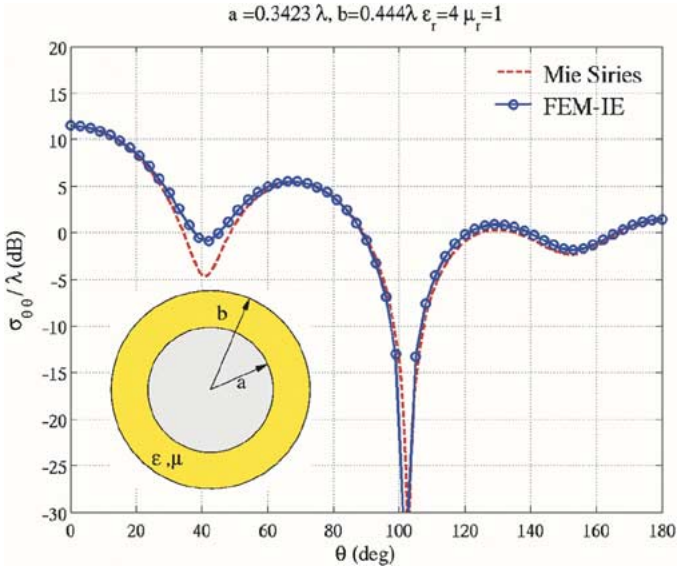

Fig. 4. Bistatic RCS of a coated dielectric sphere, at the interior resonance frequency, comparison with analytic solution.

The excitation vector blocks are given by

$$\mathbf{b}_i = \int_{S_i} \vec{w}_i(\vec{r}) \bullet \vec{J}^{\mathrm{imp}}(\vec{r}) d\Omega \quad (32)$$

$$(\mathbf{y}_M)_i = -\int_{S_i} \vec{w}_i(\vec{r}) \bullet \vec{j}^{\mathrm{inc}}(\vec{r}) d\Gamma \quad (33)$$

$$(\mathbf{y}_E)_i = \int_{S_i} \hat{n} \times \vec{w}_i(\vec{r}) \bullet \vec{E}^{\mathrm{inc}}(\vec{r}) d\Gamma. \quad (34)$$

where S_i is the finite support associated with the i^{th} basis function. Note that from all four dense submatrices $\mathbf{Q}_M$, $\mathbf{Q}_E$, $\mathbf{P}_M$, and $\mathbf{P}_E$, only one from each pair needs to be computed and stored in memory. Moreover, each submatrix is symmetric; therefore an additional factor of two can be saved.

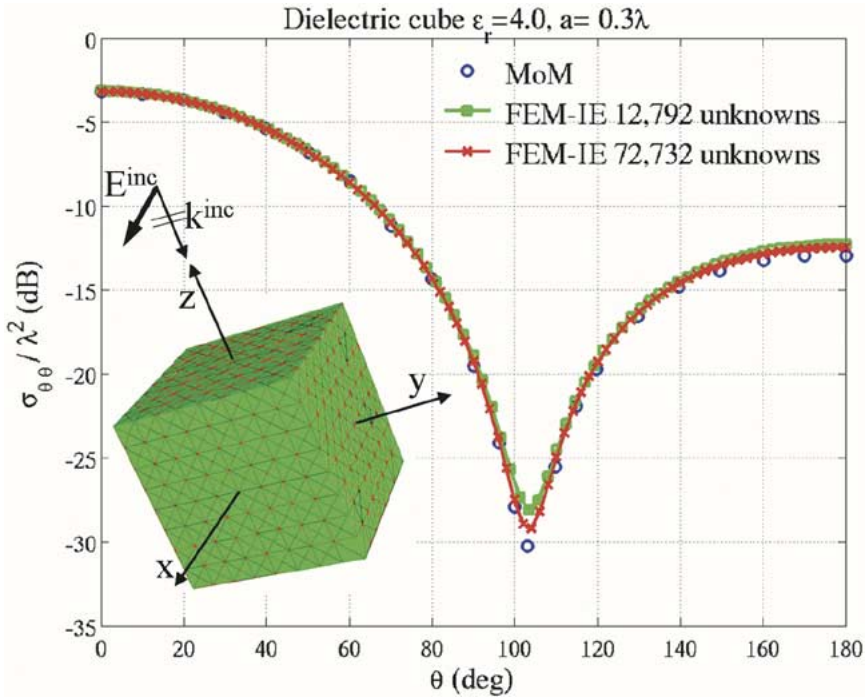

Fig. 5. Bistatic RCS of a dielectric cube on the $x-z$ plane.

III. Single Level IE-QR Algorithm

A straightforward computation of each IE submatrices in (27)–(30) will require $O(N_S^2)$ operations and memory, where N_s is the number of unknowns in the truncation surface Γ. This is a serious bottleneck especially if FEM-IE is applied in electrically large EM problems. During the last decade a number of methods have been proposed to overcome the problem. In general, most of the approaches can be classified into five categories.

1) Multipole expansion methods, like fast multipole method (FMM) [21] and multilevel FMM (MLFMM) [22], [23].
2) Panel clustering methods [24].
3) FFT based techniques, such as precorrected FFT methods [25] and adaptive integral methods (AIM) [26].
4) Wavelet based methods [27].
5) Singular value decomposition (SVD) approaches [28] or QR factorization [5].

Each method has its own advantages and shortcomings. In this work, the approach of [5] is adopted. The very reason behind, is the fact that it is the only approach that is relatively independent of Green's function, and at the same time, can be implemented in modular fashion regardless of the application, e.g., surface IE, volume IE, FEM-IE, etc. This allows for minimum modifications on the FEM-IE implementation. Moreover, it is easy to extend for applications involve multilayer media, finite number of ground planes and lossy grounds. The proposed single level IE-QR algorithm is of $O(N_S^{1.5})$ complexity for moderate size problems. In the heart of this computational reduction lies the rank deficiency of the matrix sub-blocks that correspond to well separated interactions [29]. The proposed algorithm exploits this very property of the IE equation matrix using a dual-rank revealing QR factorization. The crucial difference of the algorithm over the "conventional" textbook QR factorizations lies on the fact it *does not* require the assembly of the each matrix sub-block.

In order to avoid possible confusions among symbols in this section, $\mathbf{Q}_M$ and $\mathbf{P}_M$ will be represented by $\mathbf{Z}$, while $\mathbf{Q}$ will be reserved for the representation of the orthonormal matrix in the QR factorization. In a single level fashion, the algorithm starts with the subdivision of the triangular panels on Γ into $M = \sqrt{N_s}$ groups. The resulting inter-group interaction sub-blocks will be denoted by $\mathbf{Z}_{ij}$, where $i, j = 1, 2, \ldots, M$. Among these the self $\mathbf{Z}_{ii}$ as well as the near-field group interactions are computed as standard dense IE matrices. All the other remaining inter-group interactions are approximated by

$$\mathbf{Z}_{ij}^{m\times n} \approx \mathbf{Q}_{ij}^{m\times r} \cdot \mathbf{R}_{ij}^{r\times n} \tag{35}$$

where the superscripts denote the dimension of the group interaction matrix. In (35), r is the rank of the group interaction matrix and physically represents the amount of information required to represent the interaction with a prescribed accuracy. Without going into the details of the algorithm, which can be found in [5], the algorithm proceeds by assembling only $m \times r + n \times r$ interactions instead of $m \times n$. In reality, the rank r is only a fraction of the $\min(m, n)$.

IV. p-MUltiplicative Schwarz (p-MUS) Preconditioner

In this section a two-step preconditioner for the FEM-IE is be presented. If we denote the FEM-IE matrix of (26) by $\mathbf{K}$, the first step in the construction of the preconditioner is to extract a sparse version of $\mathbf{K}$

$$\mathbf{K}^{sp} = \begin{pmatrix} \mathbf{A} & \mathbf{C} & 0 \\ \mathbf{C}^T & \mathbf{B} + \mathbf{Q}_M^{sp} & \mathbf{D} + \mathbf{P}_M^{sp} \\ 0 & \mathbf{D}^T + \mathbf{P}_E^{sp} & \mathbf{Q}_E^{sp} \end{pmatrix} \tag{36}$$

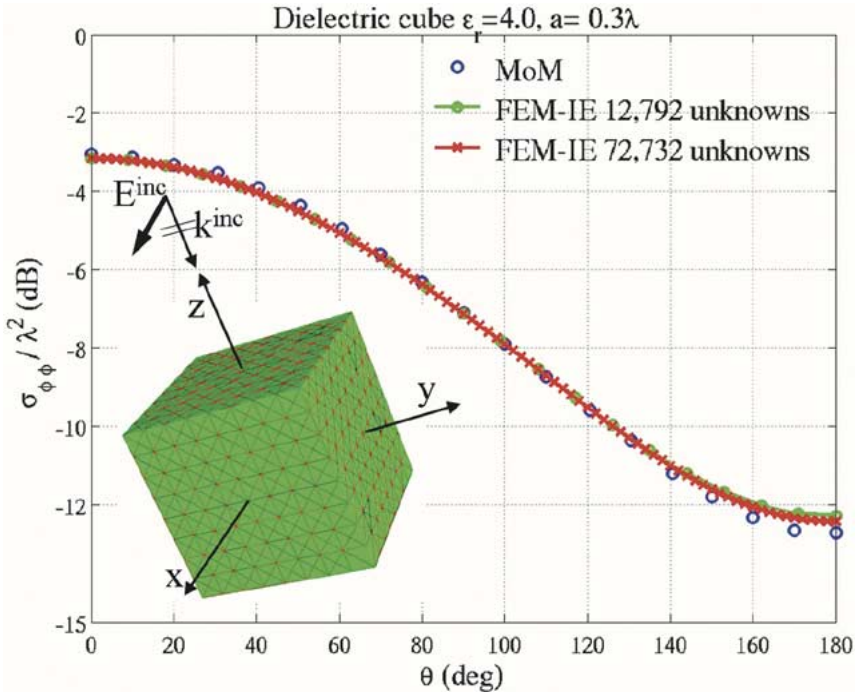

Fig. 6. Bistatic RCS of a dielectric cube in the $y-z$ plane.

where $\mathbf{Q}_M^{sp}$, $\mathbf{P}_M^{sp}$, $\mathbf{P}_E^{sp}$, and $\mathbf{Q}_E^{sp}$ are sparse versions of the corresponding dense IE matrix sub-blocks. A robust way to obtain these sparse submatrices is described in [30]. In this paper a special case of that approach is followed, by only using the FEM sparsity pattern as the "filter," namely

$$\Xi_{ij}^{sp} = \begin{cases} \Xi_{ij} & \text{iff } \mathbf{B}_{ij} \neq 0 \\ 0 & \text{elsewhere} \end{cases} \tag{37}$$

where $\boldsymbol{\Xi}$ can be either the matrix $\mathbf{Q}_M$, $\mathbf{P}_M$, $\mathbf{P}_E$, or $\mathbf{Q}_E$.

In the second stage, the p-type multiplicative Schwarz preconditioner is obtained by the Schur decomposition of $\mathbf{K}^{sp}$. Here, we present only a brief summary, the interested readers are referred to [6]–[8] for more details. First, the approximate system matrix $\mathbf{K}^{sp}$ is further divided into a 2×2 partition

$$\begin{aligned} \mathbf{K}^{sp} &= \begin{pmatrix} \mathbf{K}_{1,1} & \mathbf{K}_{1,2} \\ \mathbf{K}_{2,1} & \mathbf{K}_{2,2} \end{pmatrix} \\ &= \begin{pmatrix} \mathbf{I} & 0 \\ \mathbf{K}_{2,1}\mathbf{K}_{1,1}^{-1} & \mathbf{I} \end{pmatrix} \begin{pmatrix} \mathbf{K}_{1,1} & 0 \\ 0 & \mathbf{S} \end{pmatrix} \begin{pmatrix} \mathbf{I} & \mathbf{K}_{1,1}^{-1}\mathbf{K}_{1,2} \\ 0 & \mathbf{I} \end{pmatrix} \end{aligned} \tag{38}$$

where $\mathbf{K}_{1,1}$ and $\mathbf{K}_{2,2}$ are the first- and second-order basis function blocks, respectively. Moreover, $\mathbf{S} = \mathbf{K}_{2,2} - \mathbf{K}_{2,1}\mathbf{K}_{1,1}^{-1}\mathbf{K}_{1,2}$ is the Schur complement of $\mathbf{K}^{sp}$. From (38)

$$\begin{aligned} (\mathbf{K}^{sp})^{-1} = &\begin{pmatrix} \mathbf{I} & -\mathbf{K}_{1,1}^{-1}\mathbf{K}_{1,2} \\ 0 & \mathbf{I} \end{pmatrix} \begin{pmatrix} \mathbf{K}_{1,1}^{-1} & 0 \\ 0 & \mathbf{S}^{-1} \end{pmatrix} \\ &\times \begin{pmatrix} \mathbf{I} & 0 \\ -\mathbf{K}_{2,1}\mathbf{K}_{1,1}^{-1} & \mathbf{I} \end{pmatrix}. \end{aligned} \tag{39}$$

Note that in order to obtain the inverse of $\mathbf{K}^{sp}$, we will need to compute $\mathbf{K}_{1,1}^{-1}$ as well as $\mathbf{S}^{-1}$. Since $\mathbf{K}_{1,1}$ corresponds to the "smooth" components of the solution, according to the multigrid teaching, we shall try to obtain $\mathbf{K}_{1,1}^{-1}$ with high degree of accuracy. Therefore, we employ an incomplete Choleski factorization with drop, and set the tolerance to be 10^{-5}, namely

$$\mathbf{K}_{1,1} = \mathbf{C}_{1,1}^T\mathbf{C}_{1,1} + \mathbf{E}_1 \quad \text{where } |\mathbf{E}_1|_F \leq 10^{-5}|\mathbf{K}_{1,1}|_F. \tag{40}$$

The computation of the Schur complement inverse $\mathbf{S}^{-1}$ will be very expensive. Again, from multigrid teaching, the Schur complement corresponds to perturbation due to highly oscillating components of the solution. Thus, there is no need to account for $\mathbf{S}^{-1}$ very accurately. In the current work, we simply set

$$\mathbf{S} \approx \mathbf{K}_{2,2} = \mathbf{C}_{2,2}^T\mathbf{C}_{2,2} + \mathbf{E}_2 \quad \text{where } |\mathbf{E}_2|_F \leq 10^{-2}|\mathbf{K}_{2,2}|_F. \tag{41}$$

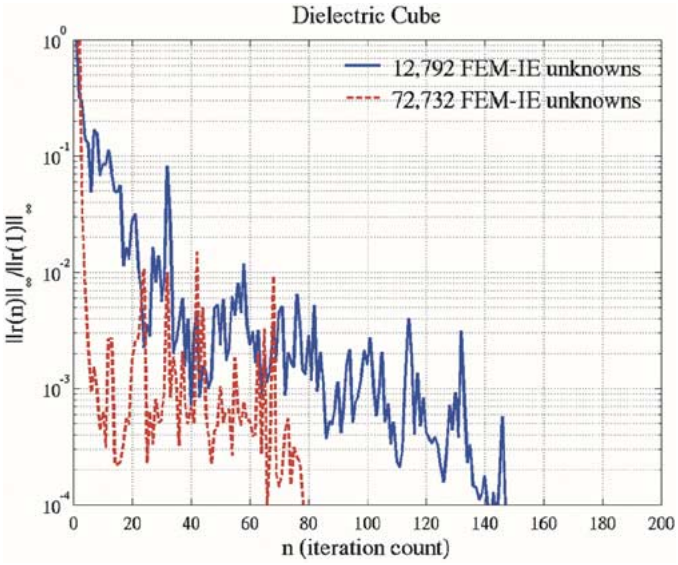

Fig. 7. Convergence of the Schwarz solver for two different discretizations of a dielectric cube.

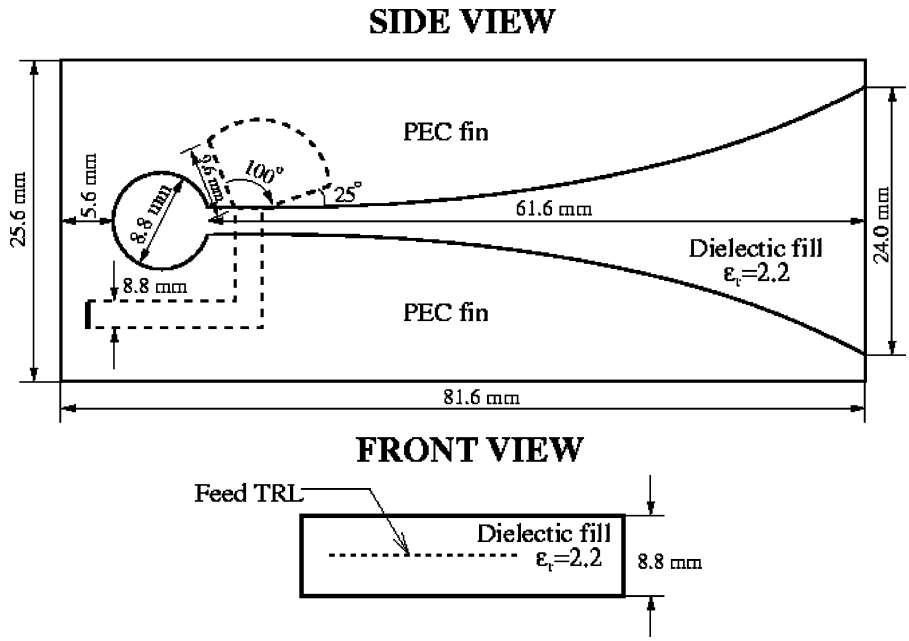

Fig. 8. Geometry, dimension, and material parameters of a single Vivaldi array elements.

If we denote the preconditioner with $\mathbf{M}$, its approximate inverse can be found from (39)–(41). Explicitly, we have

$$\mathbf{M}^{-1} \approx \begin{pmatrix} \mathbf{I} & -\left(\mathbf{C}_{1,1}^T \mathbf{C}_{1,1}\right)^{-1} \mathbf{K}_{1,2} \\ 0 & \mathbf{I} \end{pmatrix} \times \begin{pmatrix} \left(\mathbf{C}_{1,1}^T \mathbf{C}_{1,1}\right)^{-1} & 0 \\ 0 & \left(\mathbf{C}_{2,2}^T \mathbf{C}_{2,2}\right)^{-1} \end{pmatrix} \times \begin{pmatrix} \mathbf{I} & 0 \\ -\mathbf{K}_{2,1} \left(\mathbf{C}_{1,1}^T \mathbf{C}_{1,1}\right)^{-1} & \mathbf{I} \end{pmatrix}. \quad (42)$$

V. Numerical Results

Besides the rigorous mathematical framework described in [10] and [1], this symmetric coupling has not been validated through numerical experiments, yet. Numerical validations along with some other interesting results are presented in this section. Most of the comparisons will be on plane wave scattering problems. For the radiation problems the method will be pushed to the limits, and used to simulate large finite arrays.

A. Scattering

The first problem in this study consists of a $1\lambda \times 1\lambda$ plate under the incidence of a φ polarized plane wave. The plate is assumed to be infinitely thin perfect electric conductor (PEC). The truncation boundary of computational domain is placed 0.15λ away from the plate. The domain is discretized with second-order tetrahedron/triangle elements with average element size of $\lambda/6$. The accuracy of the proposed FEM-IE is compared to that of the method of moments (MoM). In Fig. 2, the monostatic RCS of the structure is plotted with solid line. In crosses is the MoM solution using an existing code; on the other hand in dashed line is the MoM solution reported in [1]. The agreement of the FEM-IE with both MoM codes is favorable over almost the entire angle spectrum. The next figure, Fig. 3, shows

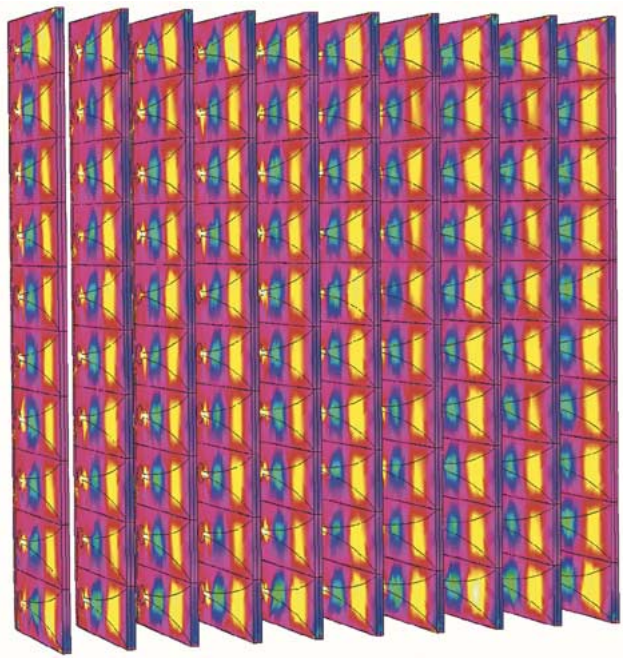

Fig. 9. Electric field distribution on the 10×10 Vivaldi array. Red and yellow indicate strong fields, whereas green indicates weak fields.

the convergence behavior of the MGCG with the pMUS preconditioner. Two different discretizations are plotted: one with 4,876 FEM-IE unknowns and one with 10,132 unknowns. In both cases, the conjugate gradient method converges in less than 50 iterations.

The second example attempts to compare the symmetric FEM-IE with an existing analytical solution. Therefore, a dielectric coated PEC sphere of $\varepsilon_r = 4.0$ and $\mu_r = 1.0$ is discretized. The PEC sphere has radius $\mathrm{a} = 0.3423\lambda$, whereas the dielectric shell $b = 0.4440\lambda$. The bistatic RCS of the geometry is depicted in Fig. 4. It is interesting to note that

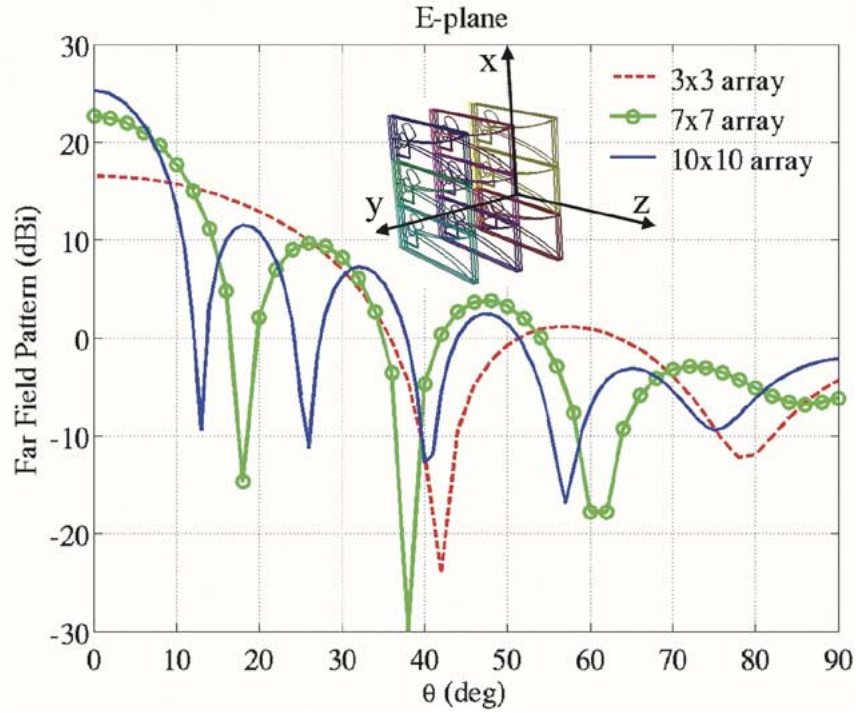

Fig. 10. E-plane far field radiation pattern for various Vivaldi arrays.

the computation is done at the "interior resonance" frequency. Nevertheless, the accuracy of FEM-IE, denoted with circles, is very good when compared with the Mie series solution in dashed line.

In the next experiment a dielectric cube geometry of $\varepsilon_r = 4.0$ and $\mu_r = 1.0$ and edge length $\mathrm{a} = 0.3\lambda$ is considered. A discretized geometry of the cube is embedded in Figs. 5 and 6, along with the incident plane wave polarization. The bistatic RCS of the configuration is plotted for the $x - z$ and $y - z$ planes in Figs. 5 and 6, respectively. Each figure compares two FEM-IE discretizations, a coarse in squares and a fine in crosses, with MoM results reported in [16]. Very good agreements are achieved, even for the coarse discretization. The convergence plots of these two different meshes are plotted in Fig. 7; the coarse grid is plotted with solid line and the fine grid with dashed line.

B. Radiation

This section presents some results obtained from the analysis of finite array radiation problems. The array configurations used in this section have been previously analyzed in [31] using the FDTD method. The interested reader is referred to that paper for a detailed description of the antenna geometric parameters.

All three arrays analyzed herein have an exponentially tapered (Vivaldi) slot element as the basic building block. Some of the element parameters are summarized in Fig. 8. The excitation of each element is done at the end of the stripline, which is denoted with a dashed line in Fig. 8. All arrays are operated at frequency $f = 5.0$ GHz, under a uniform broadside excitation. The whole array structure is backed by a finite PEC ground plane, which is placed 10 mm behind the Vivaldi elements. The finite ground plane extends approximately 0.2λ from the edge elements in each lateral direction. The elements are spaced in a $0.44\lambda \times 0.43\lambda$ uniform grid in $x - y$ plane. All three finite arrays simulated using the FEM-IE, differ only in the number of elements and the total size. The first finite array consist of a 3×3 Vivaldi elements; whereas the other two are 7×7 and 10×10 elements, respectively.

For the computational models of all three arrays, adaptive mesh refinement using absorbing boundary condition (ABC) truncation was first employed [32]. In general the meshes obtained were highly nonuniform, with elements ranging from $\lambda/8 - \lambda/12$ close to the excitation region, to $\lambda/3 - \lambda/6$ on the truncation boundary, and regions of weak field intensity. The truncation boundary was placed approximately $\lambda/4$ away from the array and finite ground plane structure. The resulting meshes were used in the symmetric FEM-IE using second-order edge elements in the FEM domain, and second-order RWG elements on the IE boundary. The resulting distribution of the magnitude of the electric field is shown in Fig. 9, for the 10×10 Vivaldi array. It is found that most of the strong fields are highly localized around the feed transmission lines and stubs. Some edge effects can be observed on the first and last row of elements, where the fields tend to be more intense. The resulting far-field radiation patterns across E and H planes are depicted in Figs. 10 and 11, respectively. In each of the figures all three 3×3, 7×7, and 10×10 arrays are plotted with dashed line, circles, and solid line respectively. More interestingly, Table I summarizes some of the computational statistics for each simulation. It is very encouraging that even without special periodicity exploitation, the brute-force application of the symmetric FEM-IE is able to solve electrically large and complicated problems with a usual PC, within reasonable time. Moreover, for these computations a double precision arithmetic was used in both setup and solution process. Among others, it should be noted that the recorded iteration number of the last column, refers to infinity

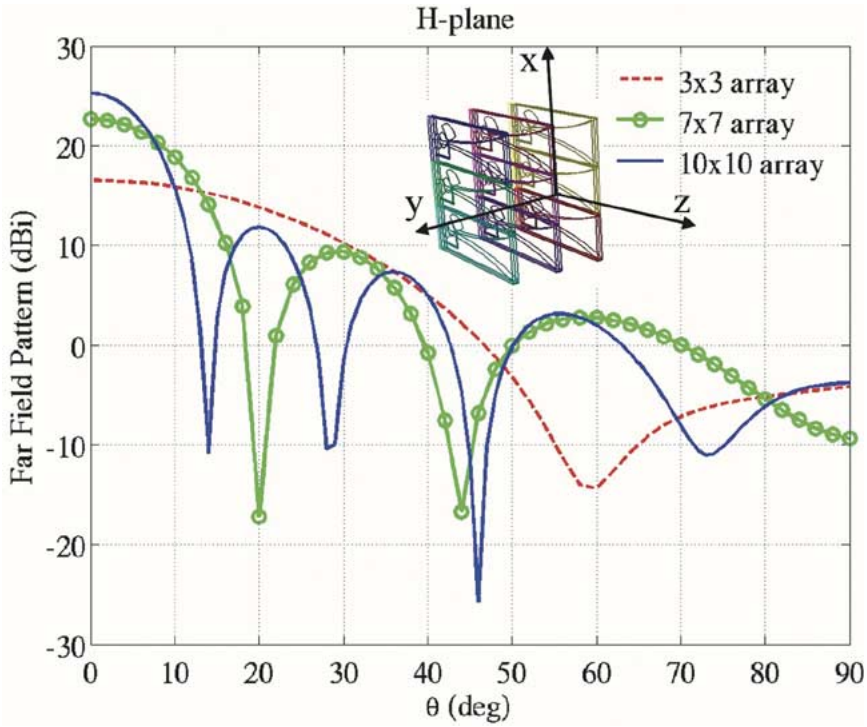

Fig. 11. H-plane far field radiation pattern of various Vivaldi arrays.

TABLE I
COMPUTATIONAL STATISTICS OF FEM-IE FOR DOUBLE PRECISION ARITHMETIC ON AN INTEL PENTIUM-IV 1.7 GHz PC

Array	L(λ)×W(λ)×H(λ)	FEM-IE unknowns	Memory (GB)	Set up time (min)	CPU time/iter. (s)	Iteration Number
3×3	1.6×1.1×1.6	80,718	0.190	19	1.9	123
7×7	3.3×3.0×1.6	528,420	0.585	40	7.4	561
10×10	4.6×4.5×1.6	1,327,790	1.452	99	20.2	1186

norm residuals of the order 10^{-3}, which is considered rather conservative for far-field computations.

VI. CONCLUSION AND LOOK AHEAD

This paper introduced a novel, for the EM community, hybrid FEM-IE method. Its uniqueness and attractiveness is in the symmetric nature of the resulting system of equations. The symmetric FEM-IE, was successfully combined with an efficient IE-QR algorithm that accelerates the overall computation of the IE portion. Furthermore, the solution process was speeded up with the adaptation of a p-type multiplicative Schwarz preconditioner. The combination of all aforementioned technologies, allowed a fast and accurate computation of challenging EM problems, on a common PC. Even though the method seems very promising much research and study need to be done yet. The single level IE-QR can be further accelerated through a multilevel algorithm. Finally, since the basis functions employed for the IE are the usual RWG basis functions, the current formulation suffers the usual low frequency instability [30]. Consequently, the number of CG iterations may increase significantly when drastically different sizes of elements exist within the same mesh. An appropriate loop-star or loop-cotree implementation will remedy this problem.

REFERENCES

[1] J.-M. Jin, *The Finite Element Method in Electromagnetics*, 2nd ed. New York: Wiley-Interscience, 2002.
[2] J. Liu and J.-M. Jin, "A novel hybridization of higher order finite element and boundary integral methods for electromagnetic scattering and radiation problems," *IEEE Trans. Antennas Propagat.*, vol. 49, pp. 1794–1806, Dec. 2001.
[3] ——, "A highly effective preconditioner for solving the finite element-boundary integral matrix equation of 3-D scattering," *IEEE Trans. Antennas Propagat.*, vol. 50, pp. 1212–1221, Dec. 2002.
[4] J.-C. Nédélec, *Acoustic and Electromagnetic Equations, Integral, Representations for Harmonic Problems*. New York: Springer-Verlag, 2001.
[5] S. M. Seo and J.-F. Lee, "A single-level low rank IE-QR algorithm for PEC scattering problems using EFIE formulation," *IEEE Trans. Antennas Propagat.*, vol. 52, pp. 2141–2146, Aug. 2004.
[6] G. Peng, "Multigrid preconditioning in solving time-harmonic wave propagation problems using tangential vector finite elements," Ph.D. dissertation, Dept. Elect. Eng., Worcester Polytechnic Institute, Worcester, MA, 1997.
[7] D. K. Sun, J. F. Lee, and Z. Cendes, "Construction of nearly orthogonal Nedelec bases for rapid convergence with multilevel preconditioned solvers," *SIAM J. Sci. Comput.*, vol. 23, no. 4, pp. 1053–1076, 2001.
[8] J. F. Lee and D. K. Sun, "pMUS (p-type Multiplicative Schwarz) method with vector finite elements for modeling three-dimensional waveguide discontinuities," *IEEE Trans. Microwave Theory. Tech.*, vol. 52, pp. 864–870, Mar. 2004.
[9] D. J. Hoppe, L. W. Epp, and J.-F. Lee, "A hybrid symmetric FEM/MOM formulation applied to scattering by inhomogeneous bodies of revolution," *IEEE Trans. Antennas Propagat.*, vol. 42, pp. 798–805, June 1994.
[10] R. Hiptmair, "Symmetric coupling for eddy current problems," *SIAM J. Numer. Anal.*, vol. 40, no. 1, pp. 41–65.

[11] M. Costabel, "Symmetric methods for the coupling of finite elements and boundary elements," in *Boundary Elements IX*, C. Brebbia, W. Wendland, and G. Kuhn, Eds. Berlin: Springer-Verlag, 1987, pp. 411–420.
[12] M. Costabel and E. P. Stephan, "Coupling of finite and boundary element methods for an elastoplastic interface problem," *SIAM J. Numer. Anal.*, vol. 27, pp. 1212–1226, 1990.
[13] H. Ammari and J.-C. Nédélec, "Couplage elements finis-èquations integrals pour la rèsolution des èquations de Maxwell en milieu hètèrogene," in *Equation aux derivees pertielles et applications. Articles dedies a Jacques-Luois Lions*. Paris: Gauthier-Villars, 1998, pp. 19–33.
[14] X. Yuan, "Three-dimensional electromagnetic scattering form inhomogeneous objects by the hybrid moment and finite element method," *IEEE Trans. Microwave Theory Tech.*, vol. 38, pp. 1053–1058, Aug. 1990.
[15] J.-M. Jin, J. L. Volakis, and J. D. Collins, "A finite-element-boundary integral method for scattering and radiation by two and three-dimensional structures," *IEEE Antennas Propagat. Mag.*, vol. 33, pp. 22–32, June 1991.
[16] X.-Q. Sheng, J.-M. Jin, J. Song, C.-C. Lu, and W. C. Chew, "On the formulation of hybrid finite-element and boundary-integral methods for 3-D scattering," *IEEE Trans. Antennas Propagat.*, vol. 46, pp. 303–311, Mar. 1998.
[17] A. Buffa, "Some numerical and theoretical problems in computational electromagnetism," Ph.D. dissertation, Dept. Math., University of Milano, Milano, Italy, 2000.
[18] E. Kreyszig, *Introductory Functional Analysis With Applications*. New York: Wiley, 1978.
[19] J.-C. Nédélec, "Mixed finite elements in R3," *Numer. Math.*, vol. 35, pp. 315–341, May 1980.
[20] A. F. Peterson, S. L. Ray, and R. Mittra, *Computational Methods for Electromagnetics*. Piscataway, NJ: IEEE Press, 1998.
[21] R. Coifman, V. Rokhlin, and S. Wandzura, "The fast multipole method for the wave equation: a pedestrian prescription," *IEEE Antenna Propagat. Mag.*, vol. 35, pp. 7–12, June 1993.
[22] J. M. Song and W. C. Chew, "Multilevel fast-multipole algorithm for solving combined field integral equation of electromagnetic scattering," *Micro. Opt. Tech. Lettt.*, vol. 10, no. 1, pp. 14–19, Sept. 1995.
[23] X.-Q. Sheng, J.-M. Jin, J. Song, W. C. Chew, and C.-C. Lu, "Solution of combined-field integral equation using multilevel fast multipole algorithm for scattering by homogeneous bodies," *IEEE Trans. Antennas Propagat.*, vol. 46, pp. 1718–1726, Nov. 1998.
[24] W. Hackbusch, *Integral Equations, Theory and Numerical Treatment*. Basel: Birkhauser-Verlag, 1995.
[25] J. R. Phillips and J. K. White, "A precorrected-FFT method for electrostatic analysis of complicated 3-D structures," *IEEE Trans. Computer-Aided Design*, vol. 16, no. 10, pp. 1059–1072, Aug. 1997.
[26] E. Bleszynski, M. Bleszynski, and T. Jaroszewicz, "AIM: Adaptive Integral Method for solving large-scale electromagnetic scattering and radiation problems," *Radio Sci.*, vol. 31, no. 5, pp. 1225–1251, May 1996.
[27] G. Beylkin, R. Coifman, and V. Rokhlin, "Fast wavelet transform and numerical algorithms," *Comm. Pure Appl. Math.*, vol. XLIV, pp. 141–183, 1991.
[28] S. Kapur and D. E. Long, "IES3: a fast integral equation solver for efficient 3-dimensional extraction," in *Proc. ICCAD 1997*, pp. 448–455.
[29] R. Kress, *Linear Integral Equations, Theory*, 2nd ed. New York: Springer-Verlag, 1999.
[30] J.-F. Lee, R. Lee, and R. Burkholder, "Loop star basis functions and a robust preconditioner for EFIE scattering problems," *IEEE Trans. Antennas Propagat.*, vol. 51, pp. 1855–1863, Aug. 2003.
[31] H. Holter and H. Steyskal, "Some experiences from FDTD analysis of infinite and finite multi-octave phased arrays," *IEEE Trans.Antennas Propagat.*, vol. 50, pp. 1725–1731, Dec 2002.
[32] D. K. Sun, Z. J. Cendes, and J. F. Lee, "Adaptive mesh refinement, h-version, for solving multiport microwave devices in three dimensions," *IEEE Trans. Magn.*, vol. 36, July 2000.

Marinos N. Vouvakis (S'99) was born in Agios Nikolaos, Crete, Greece in February 1977. He received the Diploma degree in electrical engineering, from Democritus University of Thrace (DUTH), Xanthi, Greece, in 1999 and the M.S. degree in electrical engineering from Arizona State University, Tempe, in 2001. He is currently working toward the Ph.D. degree in electrical engineering on an ANSOFT Corporation fellowship at The Ohio State University, Columbus.

In fall 1999, he joined the Telecommunications Research Center (TRC), Arizona State University, as a Graduate Research Assistant. He has been a Graduate Research Associate with the ElectroScience Laboratory, The Ohio State University, since 2002. His research interests include domain decomposition methods, finite element and integral equation methods.

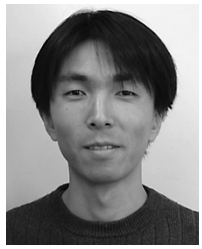

Seung-Cheol Lee was born in Seoul, Korea, on August 4, 1974. He received the B.S. degree in electrical engineering from Hong-Ik University, Seoul, in 2000 and the M.S. degree from The Ohio State University, Columbus, in 2003, where he is currently working toward the Ph.D. degree

Currently, he as an Ansoft Corporation Fellow at the ElectroScience Laboratory, Department of Electrical and Computer Engineering, The Ohio State University. His research focuses on numerical methods for waveguides, scattering, and radiation problems in electromagnetics.

Kezhong Zhao was born in Fu-Jian, China, in 1978. He received both the B.S. (*summa cum laude*) and M.S. degrees in electrical engineering from The Ohio State University, Columbus, in September 2001 and March 2003, respectively, where he is currently working toward the Ph.D. degree.

In 2001, he joined the ElectroScience Lab, The Ohio State University. His research interests include fast integral equation methods, fast hybrid FEM-MOM methods for three dimensional radiation and scattering problems, and fast domain decomposition methods.

Jin-Fa Lee (SM'99) received the B.S. degree from National Taiwan University, Taiwan, R.O.C., in 1982 and the M.S. and Ph.D. degrees from Carnegie-Mellon University, Pittsburgh, PA, in 1986 and 1989, respectively, all in electrical engineering.

From 1988 to 1990, he was with ANSOFT Corporation, where he developed several CAD/CAE finite element programs for modeling three-dimensional microwave and millimeter-wave circuits. His Ph.D. studies resulted in the first commercial three-dimensional FEM package for modeling RF/Microwave components, HFSS. From 1990 to 1991, he was a postdoctoral Fellow at the University of Illinois at Urbana-Champaign. From 1991 to 2000, he was with Department of Electrical and Computer Engineering, Worcester Polytechnic Institute. Currently, he is an Associate Professor at the ElectroScience Lab, Department of Electrical Engineering, The Ohio State University, Columbus. His current research interests are: analyzes of numerical methods, fast finite element methods, integral equation methods, hybrid methods, three-dimensional mesh generation, domain decomposition methods, and mortar finite elements.